

Supporting information

Efficient bioparticle extraction using miniaturized inertial microfluidic centrifuge

Yaohui Fang,^{1,2} Shu Zhu,^{1,2} Weiqi Cheng,¹ Zhonghua Ni,¹ and Nan Xiang,^{1*}

1. School of Mechanical Engineering, and Jiangsu Key Laboratory for Design and Manufacture of Micro-Nano Biomedical Instruments, Southeast University, Nanjing, 211189, China.

2. These authors contributed equally to this work.

**E-mails: nan.xiang@seu.edu.cn.*

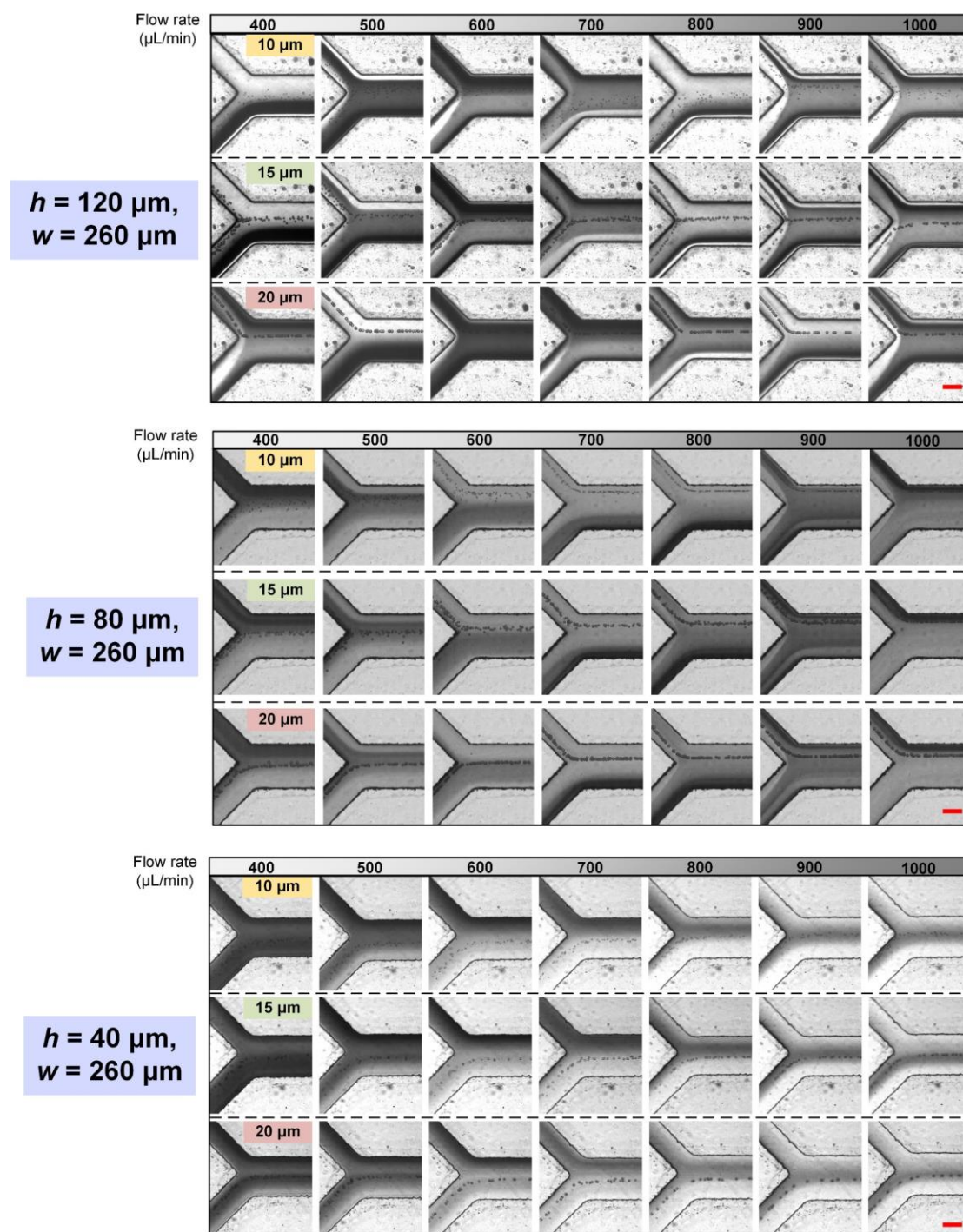


Fig.S1. Images illustrating the distributions of 10, 15, and 20 μm particles and black ink solution in inertial spiral channels with different heights at the total flow rates of 400-1000 $\mu\text{L}/\text{min}$. Scale bar is 100 μm .

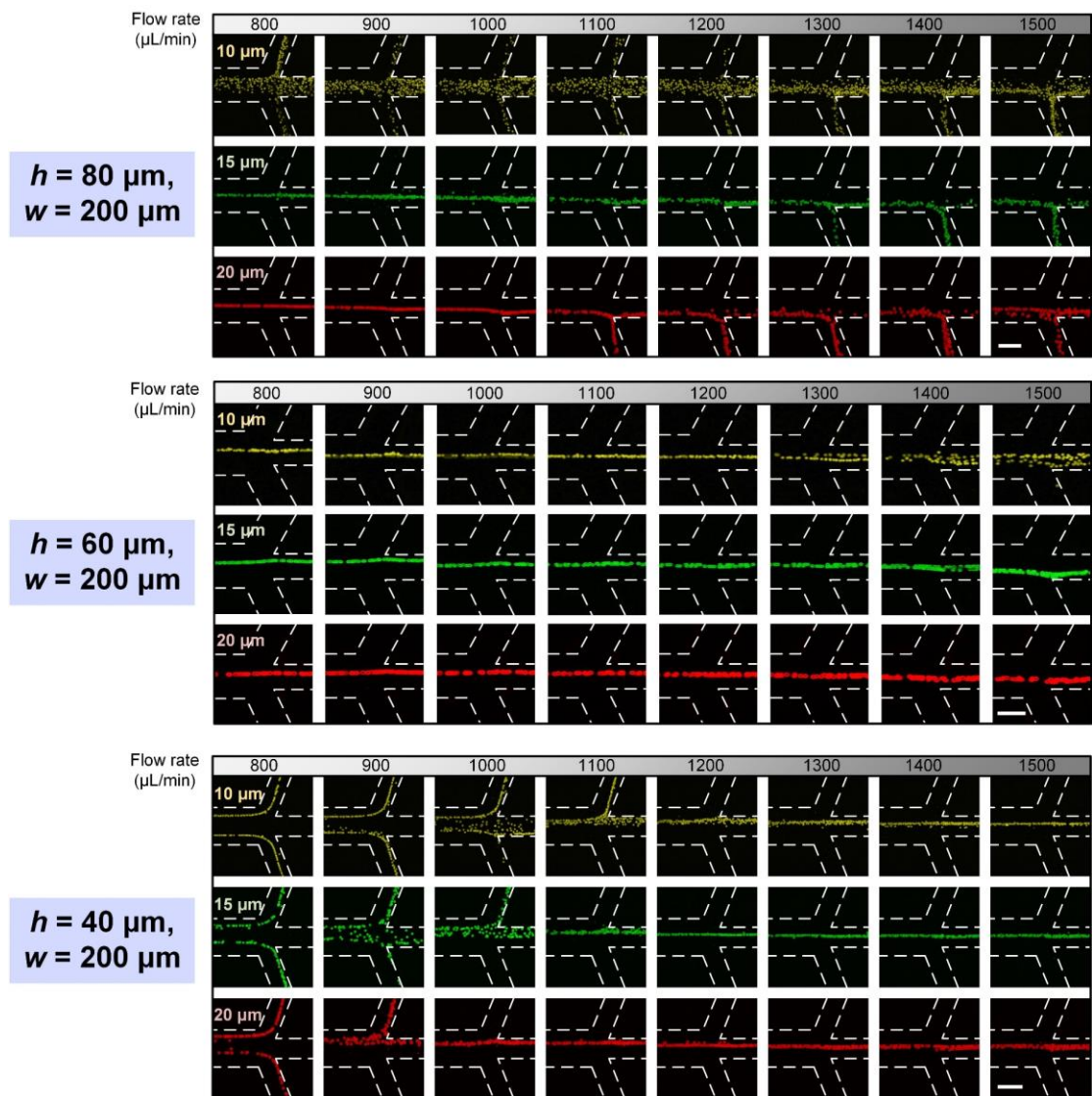


Fig.S2. Images illustrating the focusing performances of 10, 15, and 20 μm particles in inertial serpentine channels with different heights at specific flow rates of 800-1500 $\mu\text{L}/\text{min}$. Scale bar is 100 μm .

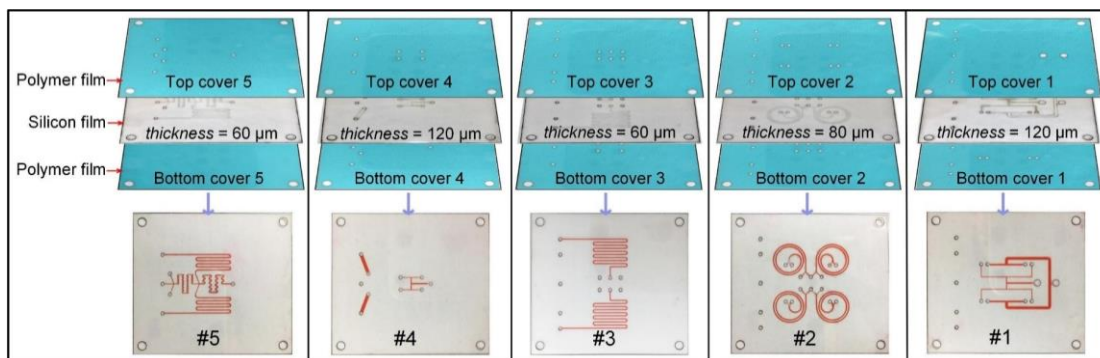


Fig.S3. Photographs and structures of different channel layers (#1-#5). A release paper (blue color) was attached with the polymer film to avoid sticking before bonding with the silicon film. Each channel is filled with red ink for clear visualization.

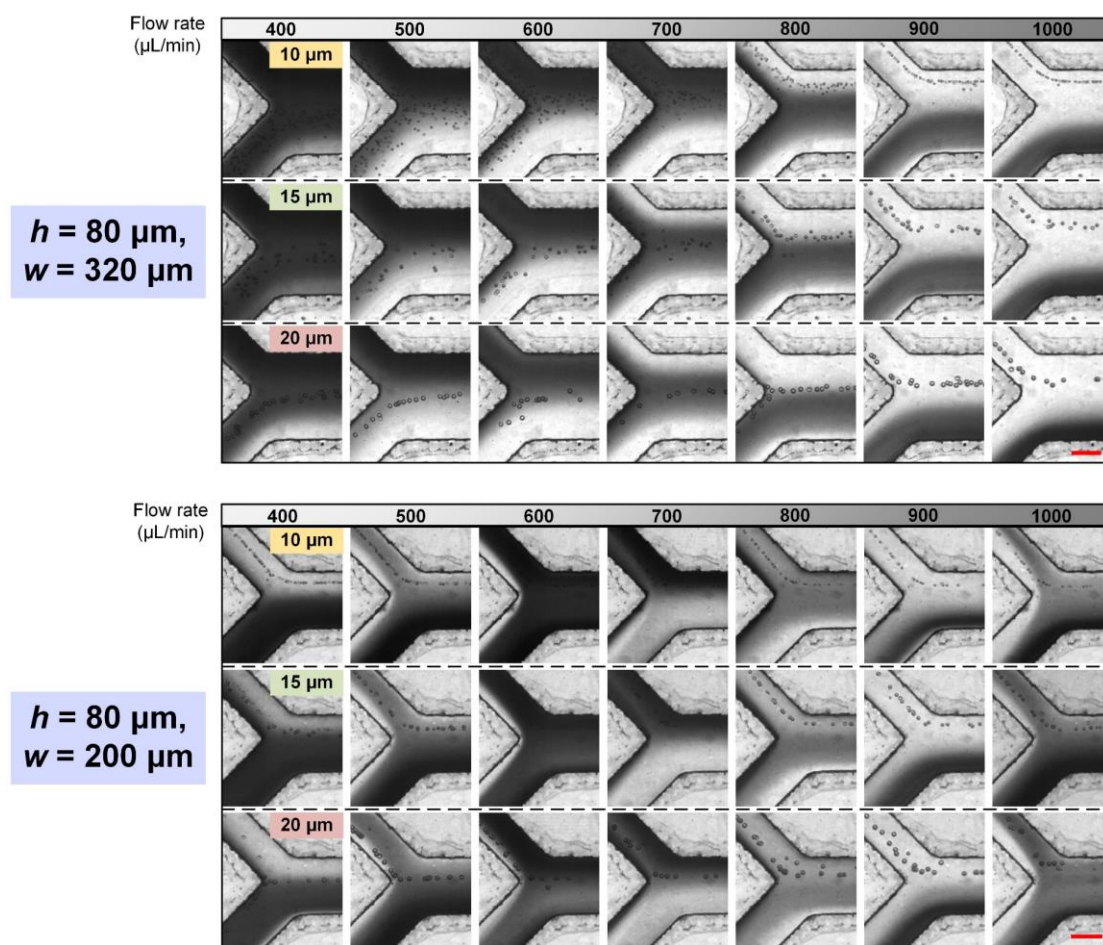


Fig.S4. Images illustrating the distributions of 10, 15, and 20 μm particles and black ink solution in inertial spiral channels with different widths at a total flow rate of 400-1000 $\mu\text{L}/\text{min}$. Scale bar is 100 μm .

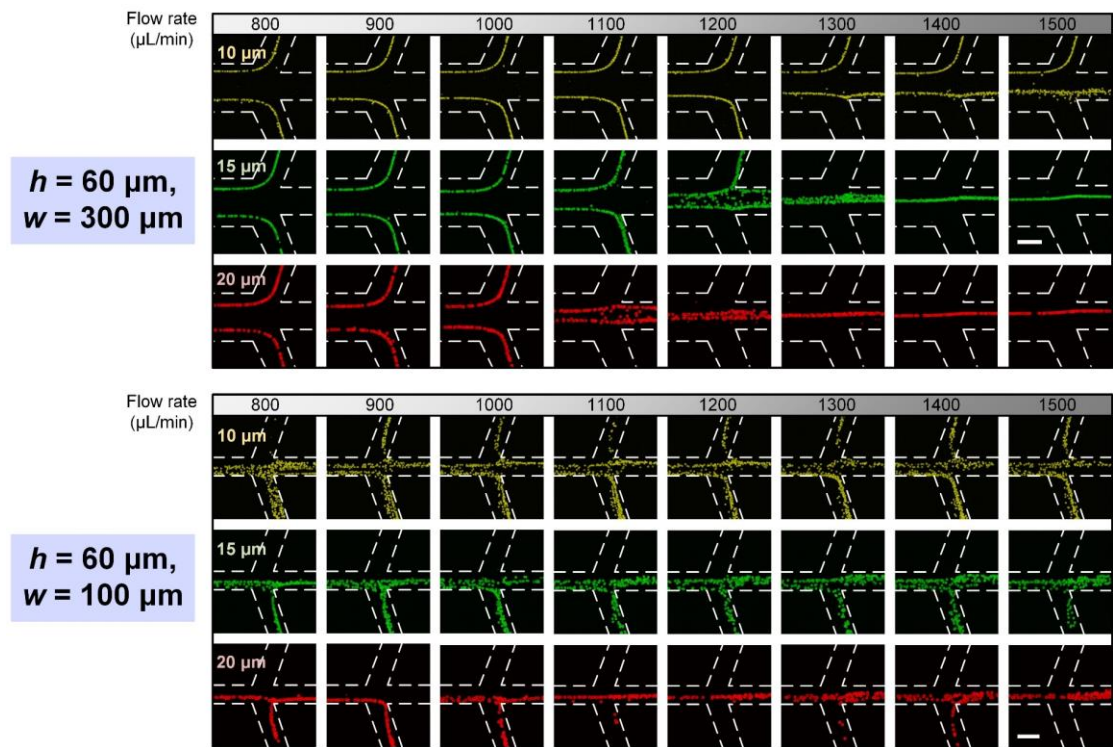


Fig.S5. Images illustrating the focusing performances of 10, 15, and 20 μm particles in inertial serpentine channels with different widths at specific flow rates of 800-1500 $\mu\text{L}/\text{min}$. Scale bar is 100 μm .

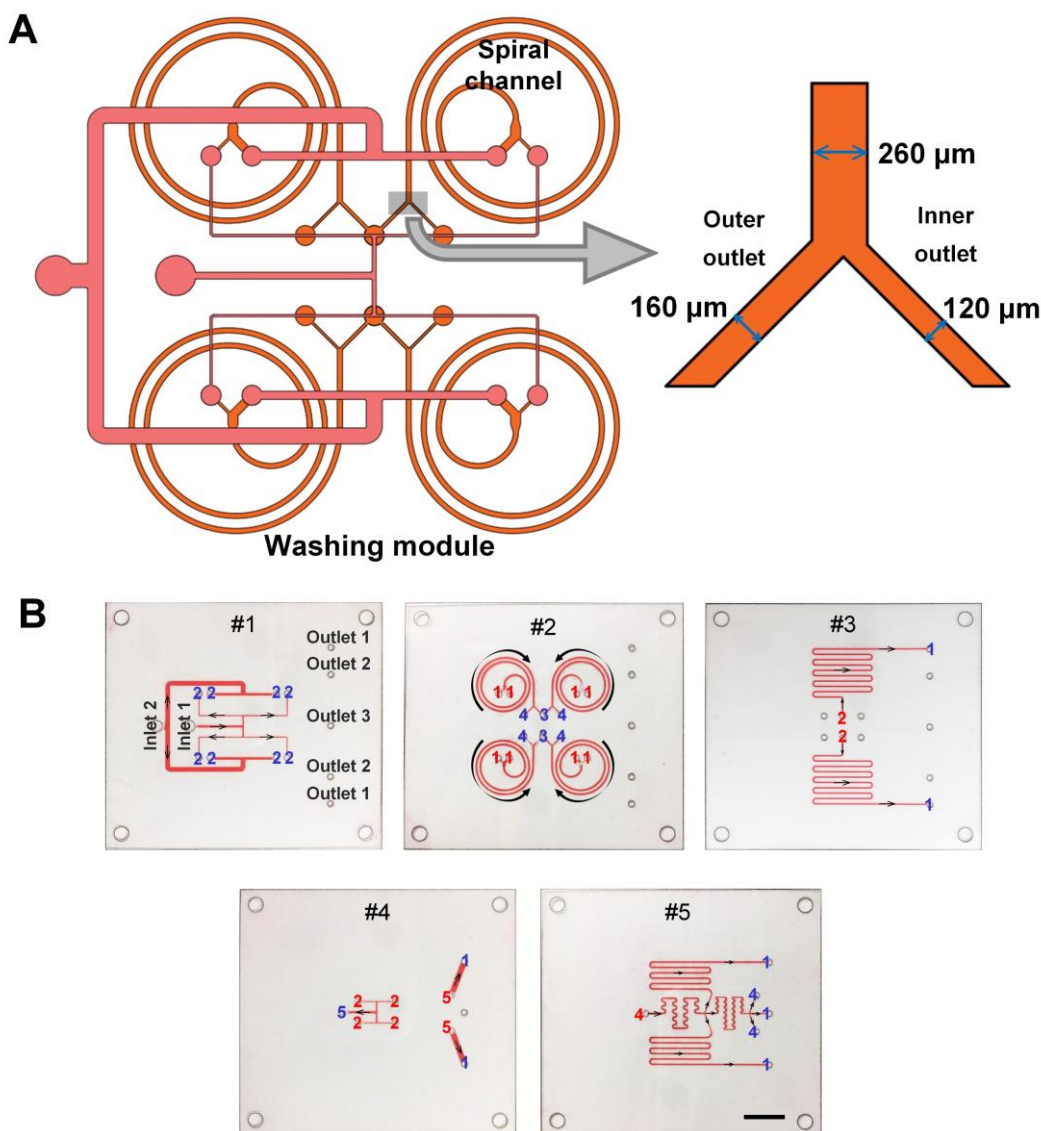


Fig.S6. (A) Schematic diagram of Y-shaped bifurcation at the end of the spiral channel. In the spiral channel, the widths of the outer and inner outlets were designed as 160 and $120\ \mu\text{m}$, separately. As the total flow rate of the spiral channel was determined as $700\ \mu\text{L}/\text{min}$, the flow rates for the outer and inner outlets were calculated to be 400 and $300\ \mu\text{L}/\text{min}$, respectively. (B) Flow paths in different layers. The black arrows represent the flow direction of the liquid. The blue number indicates the layer that liquid will flow into, while the red number indicates the layer where liquid comes from. Briefly, the liquids infused through inlets 1 and 2 were equally distributed into four spiral channels in layer #2 through flow guide channels in layer #1. The liquid from the outer outlet of each spiral channel was converged and then flowed into channels in layer #3. In addition, the liquid from the inner outlet of each spiral channel was converged through channels in layer #4, and then flowed into the channels in layer #5. Ultimately, the liquids flowed into the outlets in layer #1 through corresponding through holes in each layer. Scale bar is $1\ \text{cm}$.

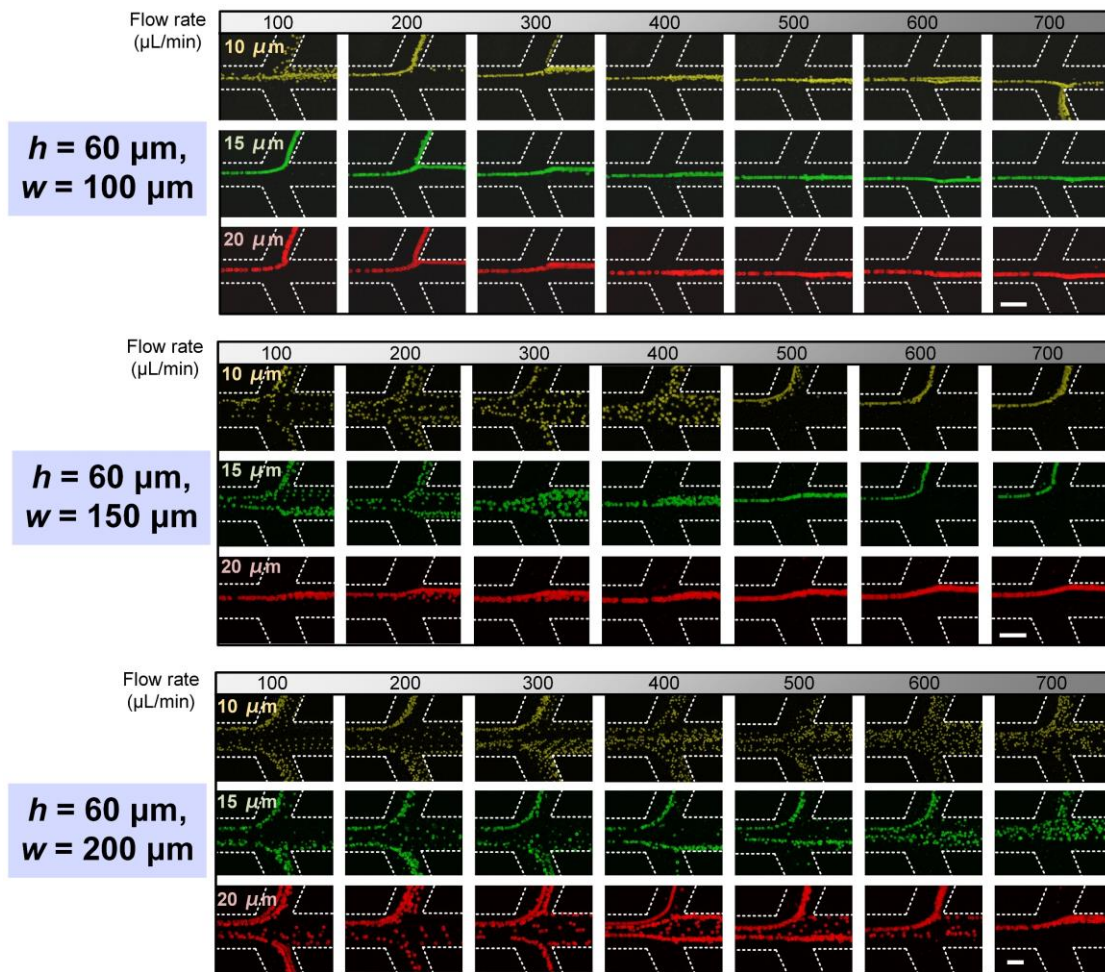
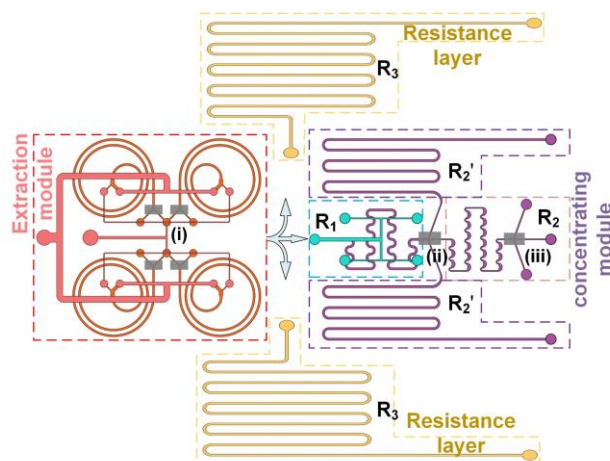
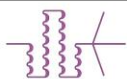
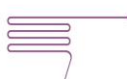
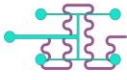


Fig.S7. Images illustrating the focusing performances of 10, 15, and 20 μm particles in the asymmetry serpentine channels with different widths at specific flow rates of 100-700 $\mu\text{L}/\text{min}$. Scale bar is 100 μm .



Channel	Flow rate ($\mu\text{L}/\text{min}$) Pressure1 = 3500 mbar	Flow rate ($\mu\text{L}/\text{min}$) Pressure2 = 4000 mbar	Flow rate ($\mu\text{L}/\text{min}$) Pressure3 = 4500 mbar	Resistance
R_2 	356.8 ± 3.1	412.5 ± 3.3	461.1 ± 2.6	9.76 ± 0.07
R_2' 	356.6 ± 4.4	408.5 ± 4.8	451.6 ± 6.4	9.85 ± 0.09
R_1 	1006.9 ± 6.5	1141.7 ± 4.6	1261.6 ± 5.5	3.51 ± 0.04
R_3 	343.1 ± 1.7	393.6 ± 5.3	442.1 ± 1.8	10.18 ± 0.02

$$R_c = R_1 + 1/3R_2$$

$$R_3 = 3/2 * (R_1 + 1/3R_2)$$

Fig.S8. Method for balancing flow resistance among each type of channels. According to the relationship between flow rate and flow resistance,¹ and the approaches for calculating parallel and series flow resistances,² the overall flow resistance for the concentrating module could be calculated as: $R_c = R_1 + 1/3R_2$, where R_c , R_1 , and R_2 are the flow resistance of the concentrating module, the first and second stage of the serpentine channel, respectively. The flow resistance of the two straight channels (R_2') in the concentrating layer were same as that of asymmetry serpentine channels. The flow resistance of the two straight resistant channels (R_3) in the resistance layer could be calculated as: $R_3 = 3/2(R_1 + 1/3R_2)$. Through the pressure-flow experiment and the flow resistance matching process, the flow resistances for R_1 , R_2 , R_2' and R_3 were calculated as illustrated in the above table.

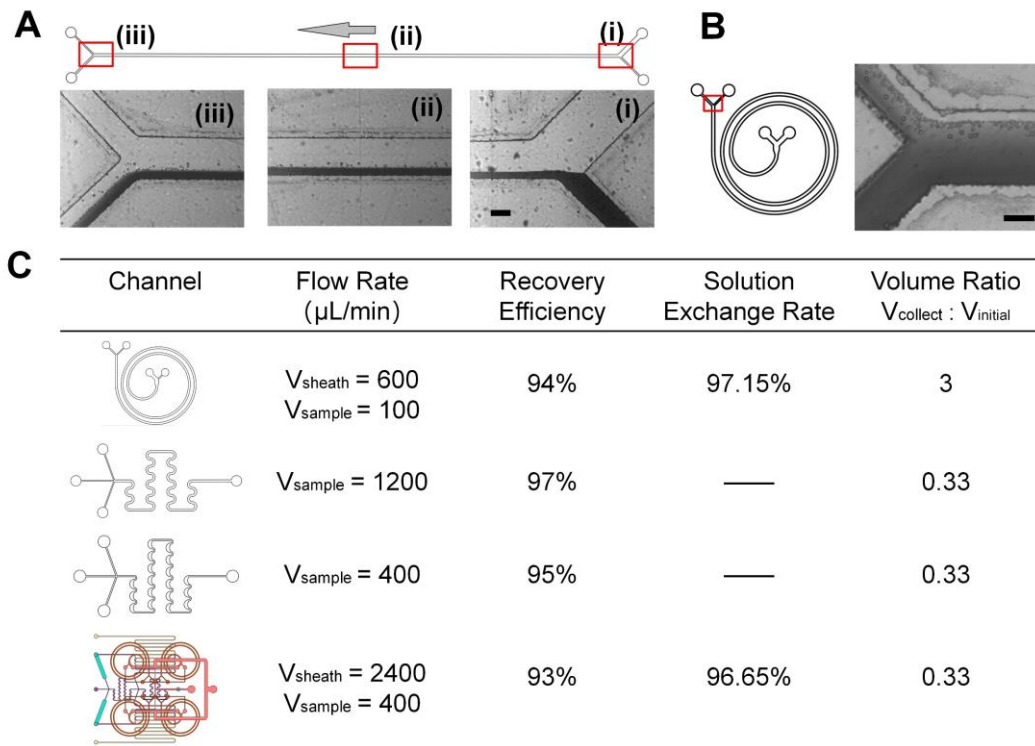


Fig.S9. (A) Images illustrating the washing effects of 10, 15, 20 μm particles using the 80 μm high, 260 μm wide, and 62.5 mm long straight channel. The distance between the focused particles and original sample was too close, which results in the impaired washing performance. (B) Images illustrating the particle washing effect for spiral channel ($h = 80 \mu\text{m}$ and $w = 260 \mu\text{m}$) under the condition that the flow rates for the two inlets were all 350 $\mu\text{L}/\text{min}$. From this image, a worse particle solution exchange rate was observed at the increased sample flow rates. (C) The comparison of the particle focusing and washing performances of single spiral and serpentine channels, as well as the integrated device. From these experiments, it was found that the spiral channel could achieve particle focusing and washing, but caused the significant volume expansion of the collected sample (3 fold). Although the symmetric or asymmetric serpentine channels could achieve particle concentrating, they could not wash particles out from the original sample. Instead, our integrated device can realize the washing and extraction of bioparticles with improved concentrations fast and automatically.

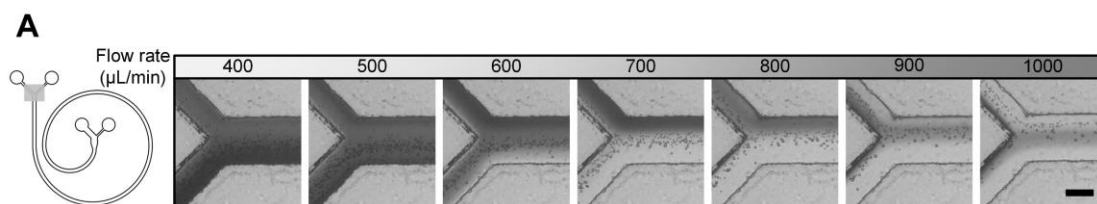


Fig.S10. Images illustrating the distributions of 10, 15, and 20 μm particles and black ink solution in inertial spiral channels with a reduced channel length (1.5 circle spiral channel) at a total flow rates of 400-1000 μL/min. Scale bar is 100 μm. The original sample was infused into the simplified spiral channel at a flow rate of 100 μL/min, while buffer solution was infused into this channel in the flow rates of 300-900 μL/min. In the total flow rates of 400-1000 μL/min, the particle was unable to be focused, and the black ink solution was unable to be separated from the particles.

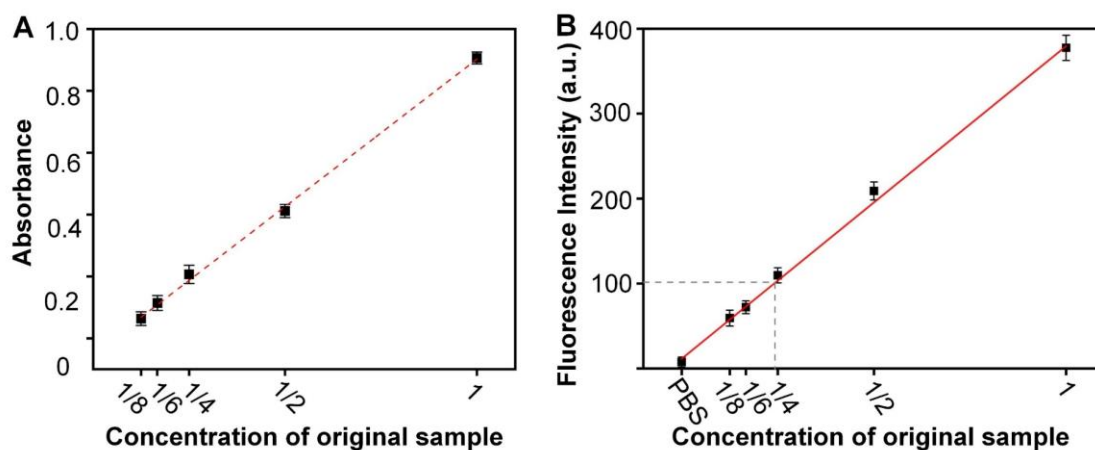


Fig.S11. Calibration curves illustrating the relationship between the absorbance and the concentration of the original culture medium (A), and the relationship between the fluorescence intensity and the concentration of the original Calcein-AM solution (B). The absorbance or fluorescence intensities of the original samples serially diluted with PBS (1/8-1 of original samples) were measured to establish the calibration curves between the absorbance or fluorescence intensities and the concentration of original samples. According to the Lambert-Beer law, the absorbance is linearly correlated with the concentration of original samples.³ According to the previous works about the fluorescence intensity of solution⁴ and our experimental results, the fluorescence intensity is proved to be linearly correlated with the concentration of original samples.

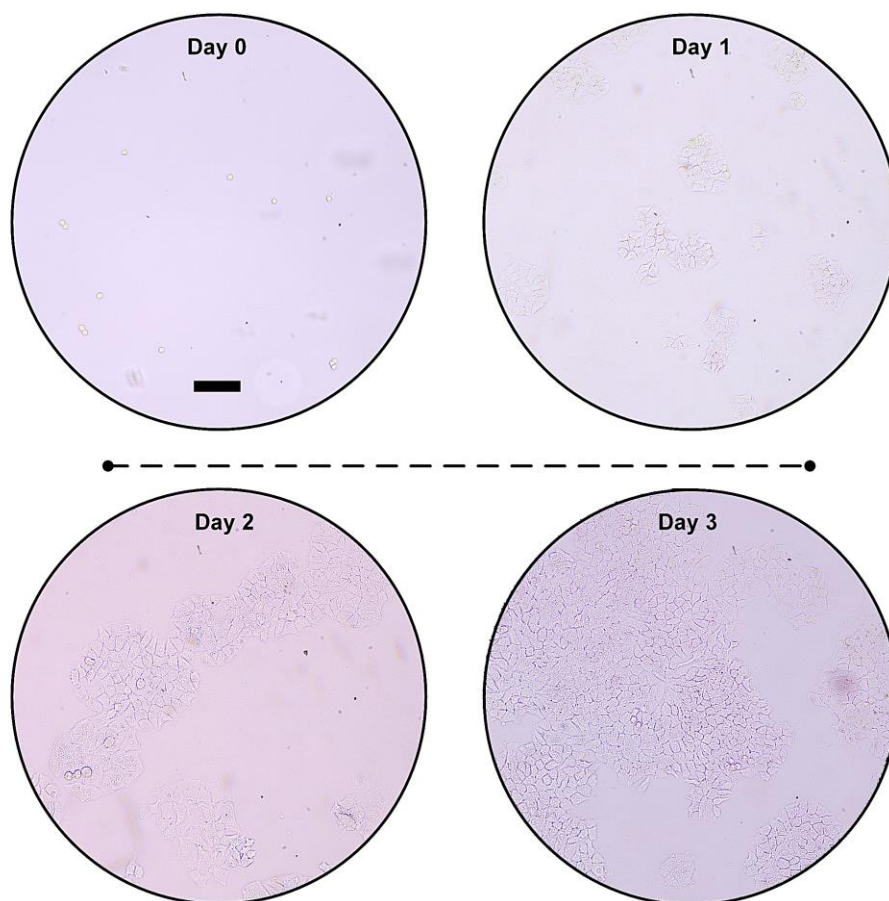


Fig.S12. Microscopic images ($10\times$) of MCF-7 cells cultured after medium exchange using our device. The cells cultured for 0, 1, 2, and 3 days illustrate a good multiplication rate, which demonstrates a good viability of cells processed by our device. Scale bar is $100\ \mu\text{m}$.

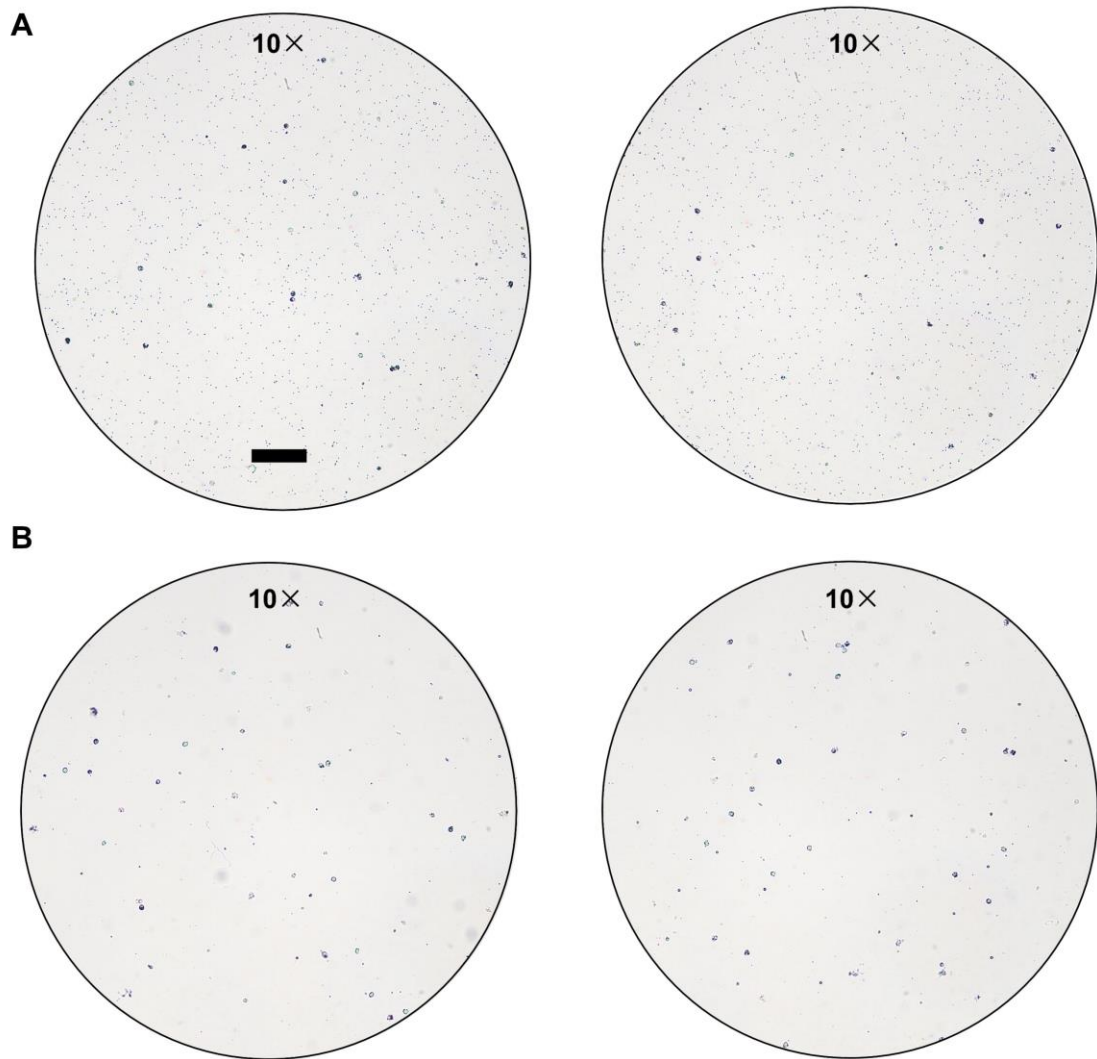


Fig.S13. (A) Microscopic images of the WBC samples labeled with magnetic beads. (B) Microscopic images of WBC samples after removing the magnetic beads. Scale bar is 100 μm .

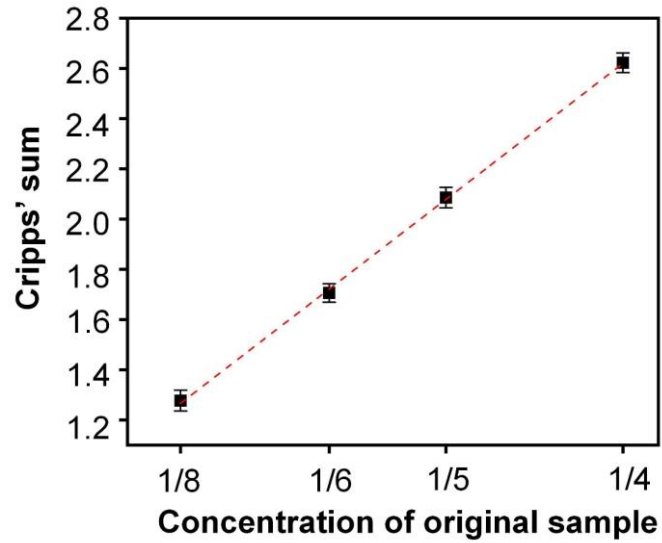


Fig.S14. Calibration curves illustrating the relationship between the Cripps' sum and the concentration of the lysed whole blood sample. The Cripps' sum is equal to $2A(576) - A(560) - A(592)$, where the $A(560)$, $A(576)$, and $A(592)$ are the absorbance measured at 560, 576, and 592 nm, respectively. The Cripps' sums for the lysed whole blood samples serially diluted with PBS (1/8-1/4 of original samples) were measured to establish calibration curves between the Cripps' sum and the concentration of original samples. The results show that the Cripps' sum is proportional to the concentration of original samples.

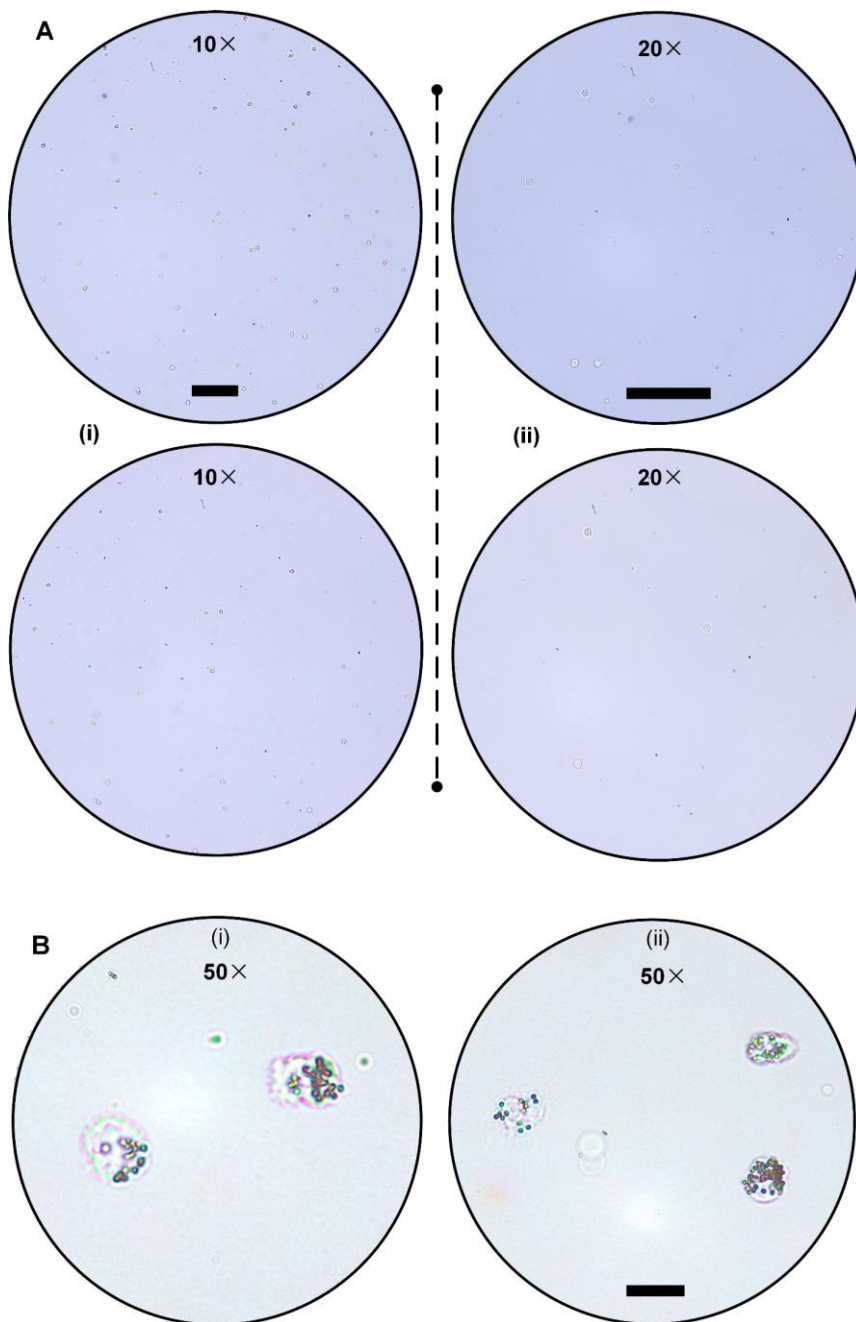


Fig.S15. (A) Microscopic images illustrating the viability of the WBCs acquired by our device ($10\times$ (i) and $20\times$ (ii)). The trypan blue exclusion test is performed to show the cell viability. The nucleus of cells with dark color illustrates the dead cells. (B) Microscopic images illustrating the cell labeling performances after being processed by our device. It was found that magnetic microbeads are well adhered on the surface of WBCs after being purified by our device. Scale bar is $100\ \mu\text{m}$.

Reference

- 1 R. M. Jack, M. M. Grafton, D. Rodrigues, M. D. Giraldez, C. Griffith, R. Cieslak, M. Zeinali, C. Kumar Sinha, E. Azizi, M. Wicha, M. Tewari, D. M. Simeone and S. Nagrath, *Advanced Science*, 2016, **3**, 1600063.
- 2 K. W. Oh, K. Lee, B. Ahn and E. P. Furlani, *Lab on a Chip*, 2012, **12**, 515-545.
- 3 M. Zude, M. Pflanz, L. Spinelli, C. Dosche and A. Torricelli, *Journal of Food Engineering*, 2011, **103**, 68-75.
- 4 D. X. Cheng, Y. H. Feng and J. L. Yan, *Microchimica Acta*, 2007, **157**, 173-179.